sustainability

MDPI

Article

The Influence of the Aggregate Configuration on the Seismic Assessment of Unreinforced Masonry Buildings in Historic Urban Areas

Valentina Cima [1,*], Valentina Tomei [2], Ernesto Grande [2] and Maura Imbimbo [2]

[1] Department of Engineering Science, University of Studies Guglielmo Marconi, Via Plinio 44, 00193 Rome, Italy
[2] Department of Civil and Mechanical Engineering, University of Cassino and Southern Lazio, Via G. Di Biasio 43, 03043 Cassino, Italy; v.tomei@unicas.it (V.T.); e.grande@unicas.it (E.G.); m.imbimbo@unicas.it (M.I.)
* Correspondence: v.cima@unimarconi.it

Abstract: Unreinforced masonry (URM) buildings in historic urban areas of European countries are generally clustered in an aggregate configuration and are often characterized by façade walls mutually interconnected with adjacent ones. As a result, the seismic performance of buildings in an aggregate configuration can be affected by the mutual interaction between the adjacent units. This interaction, often called the *aggregate effect*, could significantly influence the level of the seismic vulnerability of URM buildings in aggregate configuration toward in-plane and out-of-plane mechanisms, the latter being the object of the present paper. Traditional methods for assessing the seismic vulnerability of URM buildings neglect the interactions between adjacent buildings, potentially underestimating the actual vulnerability. This study aims to derive fragility curves specific for UMR buildings in aggregate configuration and proposes an innovative methodology that introduces the *aggregate effect* into an analytical approach, previously developed by the authors for isolated URM buildings. The *aggregate effect* is modeled by accounting for the friction forces arising among adjacent facades during the development of out-of-plane overturning mechanisms by considering different scenarios, based on how façade walls interact with neighboring structures (e.g., whether they are connected to transverse and/or lateral coplanar ones). The proposed approach is applied to a real case study of an Italian historical center. The obtained results demonstrate that the *aggregate effect* significantly influences the fragility curves of URM buildings arranged in aggregate configurations. This highlights the importance of considering this effect and the usefulness of the proposed approach for large-scale assessments of seismic vulnerability in historic urban areas, contributing to sustainable disaster risk prevention.

Keywords: aggregate effect; building in aggregate; unreinforced masonry; out-of-plane mechanisms; historic urban area; fragility curves

Citation: Cima, V.; Tomei, V.; Grande, E.; Imbimbo, M. The Influence of the Aggregate Configuration on the Seismic Assessment of Unreinforced Masonry Buildings in Historic Urban Areas. *Sustainability* **2024**, *16*, 4172. https://doi.org/10.3390/su16104172

Academic Editor: Constantin Chalioris

Received: 29 March 2024
Revised: 6 May 2024
Accepted: 14 May 2024
Published: 16 May 2024

1. Introduction

In many European countries, historic urban areas are generally characterized by unreinforced masonry (URM) buildings commonly clustered in aggregated configurations [1–5]. These buildings, due to their construction and evolution history, were not built in a unique phase but they were gradually 'assembled' over time through a process of merging, expanding, and modifying the original structures. As a result, within a building aggregate, it is possible to delineate sections of buildings characterized by top-to-bottom structural continuity. These sections, termed structural units (S.U.s) [6,7], typically arise from a unified construction process or the presence of homogeneous vertical and horizontal elements, which facilitate a uniform distribution of loads. They can be classified into three main categories on the basis of their construction genesis: pre-existing, growth, and saturation S.U.s (see Figure 1). The pre-existing units are those that were originally built as individual buildings before being incorporated into the aggregate; the growth units are those that were

added to the pre-existing units; the saturation units are those that fill the gaps between pre-existing and/or growth units.

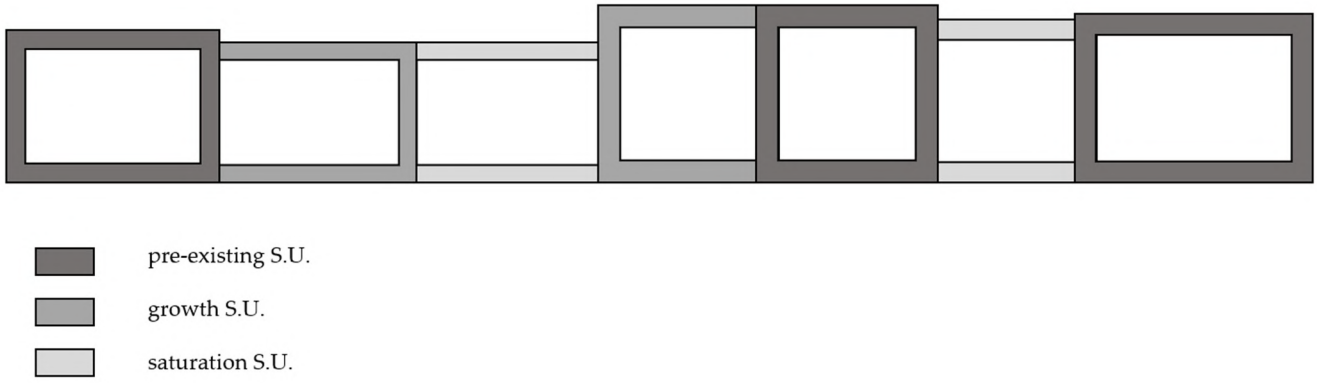

Figure 1. Graphical representation of a building aggregate with its S.U.s.

The above features contribute to the complexity of assessing the seismic vulnerability of aggregate complexes, especially because the façade walls of the different S.U.s are often interconnected with each other and transmit mutual forces due to these connections, creating mutual interactions among the adjacent structures. The effect of these interactions, referred to as the *aggregate effect* [1,8–10], can affect the seismic behavior of the single S.U.s that make up the aggregates. Consequently, during an earthquake, each S.U. does not behave as an isolated entity but it is affected by the presence of adjacent structures.

Recent earthquakes in Croatia [11], Greece [12], and Italy [5,13–16] have again highlighted the significant threat posed by seismic events to historic urban area. The consequences of earthquakes in these areas profoundly impact both residents' safety and the economies of the affected countries [17,18]. Improving the safety of such areas poses a crucial challenge, requiring sustainable solutions to minimize waste and energy consumption.

In recent years, numerous studies have addressed the seismic vulnerability of aggregate buildings in historic urban areas [3,4,19–26]. Some of them propose approaches at various scales, such as single aggregate buildings or on a territorial scale [27,28]. For example, in [29], the historic center of Campotosto (central Italy) is analyzed on an urban scale by using an empirical method based on data relevant to the post-2009 L'Aquila earthquake, as well as being analyzed on a building aggregate scale by applying an analytical method implemented in the Vulnus software [30]. Similarly, in [28], the historical center of Castelpoto (southern Italy) is analyzed on an urban scale by applying the vulnerability index method [31] and taking into account the interactions between adjacent structures, as proposed in [32,33], as well as being analyzed at the building aggregate scale by means of the 3Muri software [34].

Among approaches operating at the territorial scale, fragility curves are the most commonly used tool; they enable the assessment of seismic vulnerability of buildings or parts of buildings in probabilistic terms as the seismic intensity varies [35,36]. In particular, several methods are available in the current literature for defining fragility curves for aggregate buildings in historic centers. These methods are based on empirical [22], analytical [2,37–41], and hybrid approaches [42–44]. In this context, one of the main and still open issues regards the evaluation of the so-called *aggregate effect* on the fragility curves for out-of-plane mechanisms, which could play a crucial role in the vulnerability of historic buildings at urban scales.

The present paper aims to introduce the *aggregate effect* in the derivation of fragility curves for URM buildings in aggregate configuration prone to out-of-plane overturning mechanisms of their façade walls. In particular, this study proposes a new approach that, starting from a previous proposal of the authors [45–47], specifically takes into account the *aggregate effect*. This is achieved by considering, in the analysis of the mechanisms, the different friction actions that may occur at the intersections between the façade wall of

the building under consideration and the walls of the adjacent buildings. These actions are evaluated assuming that there is a partially effective connection between the façade wall and the transverse walls and/or coplanar façade walls of adjacent S.U.s, due to the presence of interconnecting blocks.

The novelty of the proposed approach is the introduction of the aggregate effect into the process for deriving the fragility curves. Currently, existing methods assess the fragility toward out-of-plane actions of URM buildings by disregarding the effect of neighboring S.U.s and considering them as isolated buildings. This assumption could lead to an underestimation of the seismic vulnerability of URM aggregate buildings. To address this limitation, this study incorporates the *aggregate effect* of adjacent buildings into the fragility analysis, offering a more comprehensive assessment of the seismic performance of URM buildings in aggregate configuration.

Specifically, the fragility curves of the S.U.s that make up a building aggregate of an urban historical area are derived as a function of the number of floors and the most probable out-of-plane mechanism in case of an earthquake. Thus, the information obtained from the application of the proposed procedure makes it possible to identify the most vulnerable S.U.s within an aggregate, providing engineers and administrations with useful information for prioritizing interventions and allocating the necessary resources. On the other hand, the findings can help authorities to develop evacuation plans and emergency response strategies in historic areas.

Aligned with the disaster prevention topic of this Special Issue, which aims to reduce the gap between researchers, decision-makers, and stakeholders in the process of disaster risk reduction, the proposed approach would enhance the safety of historic urban areas through the use of reliable approaches for seismic vulnerability assessment. These approaches could facilitate the sustainable management of pre-earthquake interventions, thereby reducing costs and environmental impacts associated with post-interventions, which tend to have a greater environmental footprint.

It is pointed out that, given the high susceptibility of historic buildings to out-of-plane overturning modes involving their façades, as reiterated by recent earthquakes in Italy [5,13–16], this study focuses on the overturning mechanisms affecting the entire façade (global simple overturning), those limited to the upper levels (partial overturning), and those involving the portion of the wall from bottom to top between façade openings (global simple overturning along openings).

The proposed procedure is then applied to a real case study located in central Italy, in order to assess the vulnerability of its recurring building typologies. The obtained results demonstrate the usefulness of the proposed procedure for assessing the vulnerability of historic urban areas and highlight the influence of the *aggregate effect*, indicating which construction details have the greatest impact on this effect.

This paper is structured into three parts. After a general introduction, Section 2 describes the different types of connection that can occur between URM buildings in aggregate configuration and how the *aggregate effect* is modeled. Then, Section 3 presents the proposed approach for the derivation of the fragility curves, illustrating how to incorporate the *aggregate effect* analyzed in Section 2. Finally, Section 4 describes the application of the approach to a real case study and analyzes the obtained results.

2. Aggregate Effect

The *aggregate effect* acting among contiguous S.U.s is introduced by referring, as an example, to the aggregate depicted in Figure 2, in which the central S.U. is built in adherence with the adjacent ones by sharing the boundary walls.

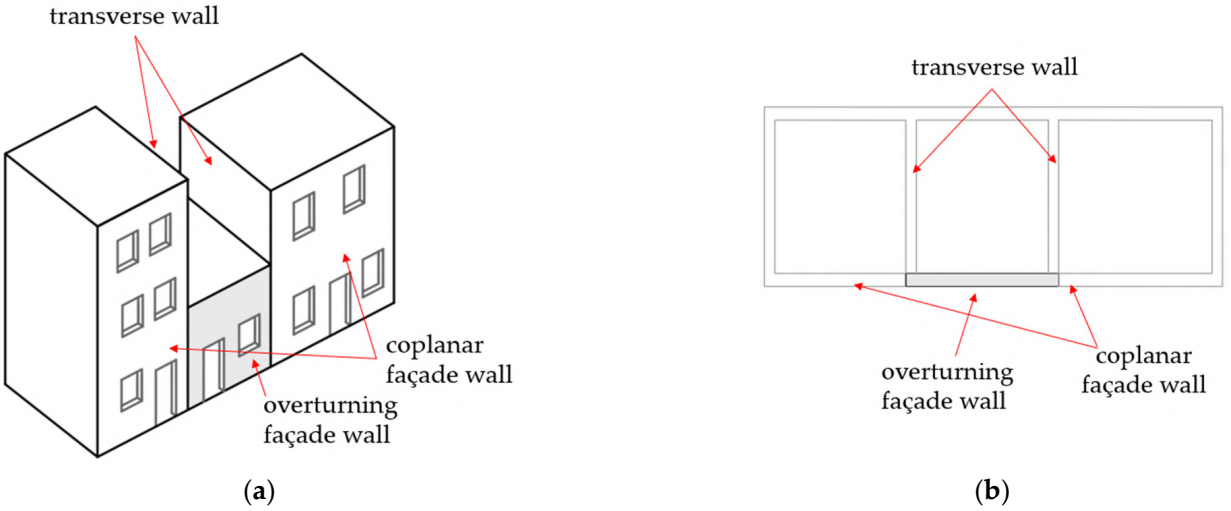

Figure 2. Sketch of the typical building aggregate considered in the study: (**a**) axonometric view; (**b**) plan.

Generally, the connection of the façade wall of the central S.U. with the transverse walls and/or the coplanar façade walls of the adjacent S.U.s (Figure 2a,b) can be of three possible types:

1. Good connection;
2. Ineffective or absent connection;
3. Partial connection.

In the first case, it is unlikely that the façade wall could experience simple out-of-plane overturning mechanisms (global or partial). However, it might be subjected to other failure mechanisms, such as horizontal or vertical bending mechanisms when thrusts of arches, vaults, and roofs act along its orthogonal direction, and compound overturning mechanisms when the façade wall is part of a corner S.U. of the aggregate.

In the second and third cases, the façade wall can be susceptible to global or partial overturning mechanisms, provided that there are no devices, such as curbs and chains, that prevent the wall's overturning mechanisms. In particular, in the second case, the façade wall is not affected by any interactions with the adjacent buildings and can be considered in an isolated configuration; in the third case, it is assumed that the wall is affected by the interactions with the adjacent buildings to which it is connected, which are referred to as the *aggregate effect*.

Based on the above considerations, this study models the *aggregate effect* by considering the frictional forces acting at the connections between the overturning façade wall and the transverse walls, shared with the adjacent units, and/or the coplanar façade walls of the adjacent units [9,47]. It is assumed that the overturning façade wall is interconnected with the transverse adjacent walls through parallelepiped interconnecting blocks, such as those illustrated in Figure 3. Although URM can be made up of irregularly shaped blocks, the simplification of considering regular parallelepiped interconnecting blocks enables the simulation of frictional contact between facade wall blocks embedded in adjacent walls. This representation effectively captures the global *aggregate effect* without introducing overly complex shapes that would affect the computation effort of the approach.

In this scenario, the friction force acts at the overlapping surface between the blocks. For brevity, in the following, the overlapped portion of the block where the friction acts is named "semi-blocks".

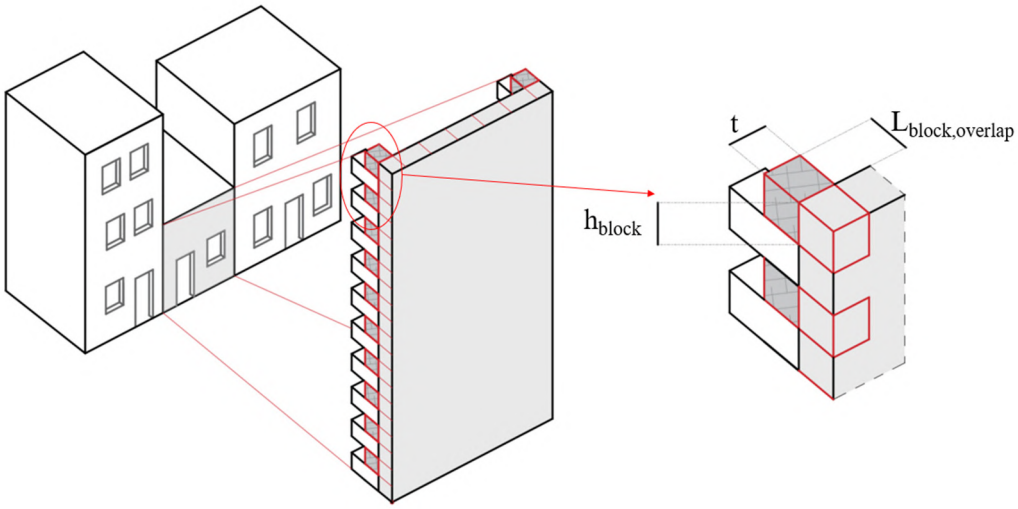

Figure 3. Interconnecting blocks.

In particular, the resultant friction forces on both the sides of the wall, F, are the sum of two components, F_b and F_q, defined as follows:

- F_b is the result of friction forces, f_i, generated by the weight of the individual semi-block (see Figure 4a).
- F_q is the result of friction forces due to the overloads (Q_i) acting on the interconnection semi-blocks due to two contributions: the weight of the portion of the wall of the adjacent building placed above the semi-blocks (shown by way of example with the cyan outline in Figure 4b) and the loads of the slabs of both the unit itself and adjacent units (refer to Figure 4b, where the loads acting on the semi-blocks are illustrated under the assumption that the slabs of adjacent units are perpendicular to the facades. Consequently, these loads do not exert an effect on the transversal semi-blocks).

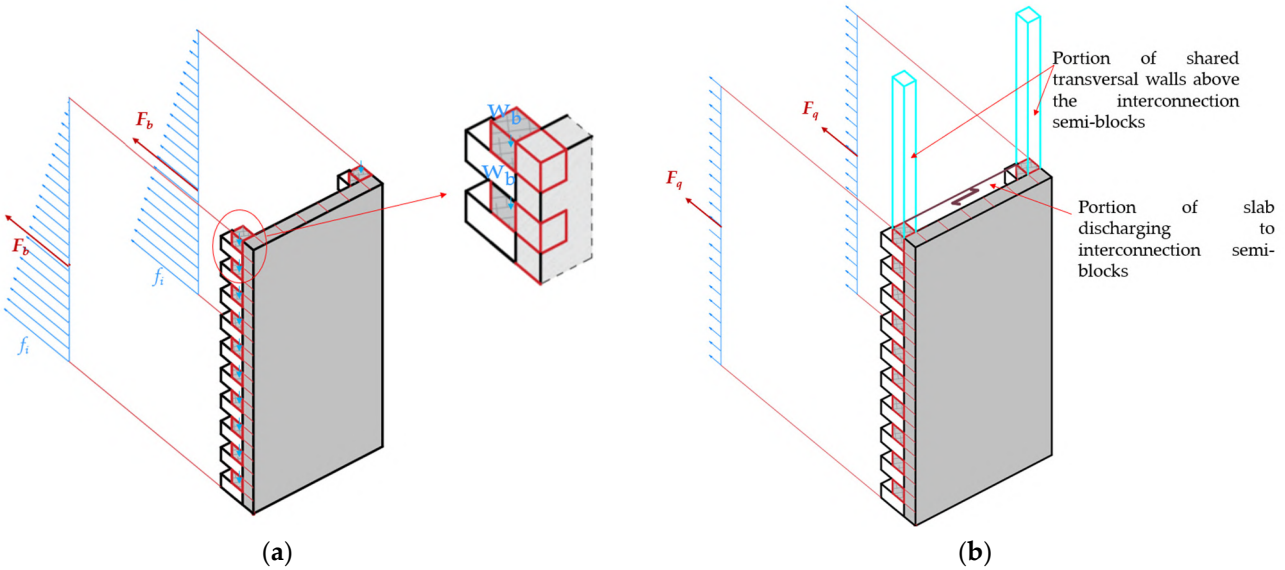

Figure 4. Distribution of the friction forces due to (**a**) the weight (w_b) of the interconnecting semi-blocks; (**b**) the overloads acting on the semi-blocks in the hypothesis that the slabs of adjacent units are perpendicular to the façades.

Equations (1) and (2) provide the formulas for calculating F_b and F_q [47–49]:

$$F_b = \sum_{i=1}^{n} f_i = \mu \cdot w_b \cdot n \cdot \frac{(n+1)}{2} \quad (1)$$

$$F_q = \mu \cdot \sum_{i=1}^{n} Q_i \quad (2)$$

In Equations (1) and (2), the following can be noted:

- f_i is the friction force acting at each semi-block and due to the weight of the individual semi-block (see Figure 4a);
- μ is the friction coefficient between the interconnecting blocks [50];
- n is the number of rows of interconnecting blocks, equal to the ratio between the height of the overturning wall and the height of the interconnecting block;
- w_b is the weight of the generic interconnection semi-block (see Figure 4a), given by the following formula:

$$w_b = \gamma_m \cdot t \cdot h_{\text{block}} \cdot L_{\text{block,overlap}} \quad (3)$$

where γ_m is the masonry specific weight, h_{block} and t are, respectively, the block height and thickness, and $L_{block,overlap}$ is the length of the semi-blocks (see Figure 3).

- Q_i represents the overloads acting on the interconnecting semi-blocks, due to two contributions: the weights of the portions of the wall of the adjacent buildings placed above the blocks and the loads of the slabs of both the unit itself and adjacent units. It is worth noting that in historical centers, the units that make up a building aggregate can frequently have different floor heights and numbers of floors, as shown in Figure 5, and they may have some floors with slabs aligned parallel to the façades and others with slabs perpendicular to the façades.

Figure 5. Example of building aggregate with S.U.s having different numbers of stories and staggered slabs.

Within the different possible connection scenarios characterizing an aggregate, this study considers six scenarios (see Figure 6), identified by the following labels "ac ij", where "i" indicates the number of side walls connected to the adjacent S.U.s (1 or 2), while "j" indicates the type of adjacent wall involved in the connections: it is equal to "T" in case of connection with the transverse wall and equal to "L" in case of connection with the lateral coplanar wall:

- Scenario "ac 1T"—the façade wall is partially connected to the transverse walls on one side (Figure 6a);

- Scenario "ac 2T"—the façade wall is partially connected to the transverse walls on both sides (Figure 6b);
- Scenario "ac 1L"—the façade wall is partially connected to the lateral coplanar walls on one side (Figure 6c);
- Scenario "ac 2L"—the façade wall is partially connected to the lateral coplanar walls on both sides (Figure 6d);
- Scenario "ac 1TL"—the façade wall is partially connected to both the transverse and lateral coplanar walls on one side (Figure 6e);
- Scenario "ac 2TL"—the façade wall is partially connected to both the transverse and lateral coplanar walls on both sides (Figure 6f).

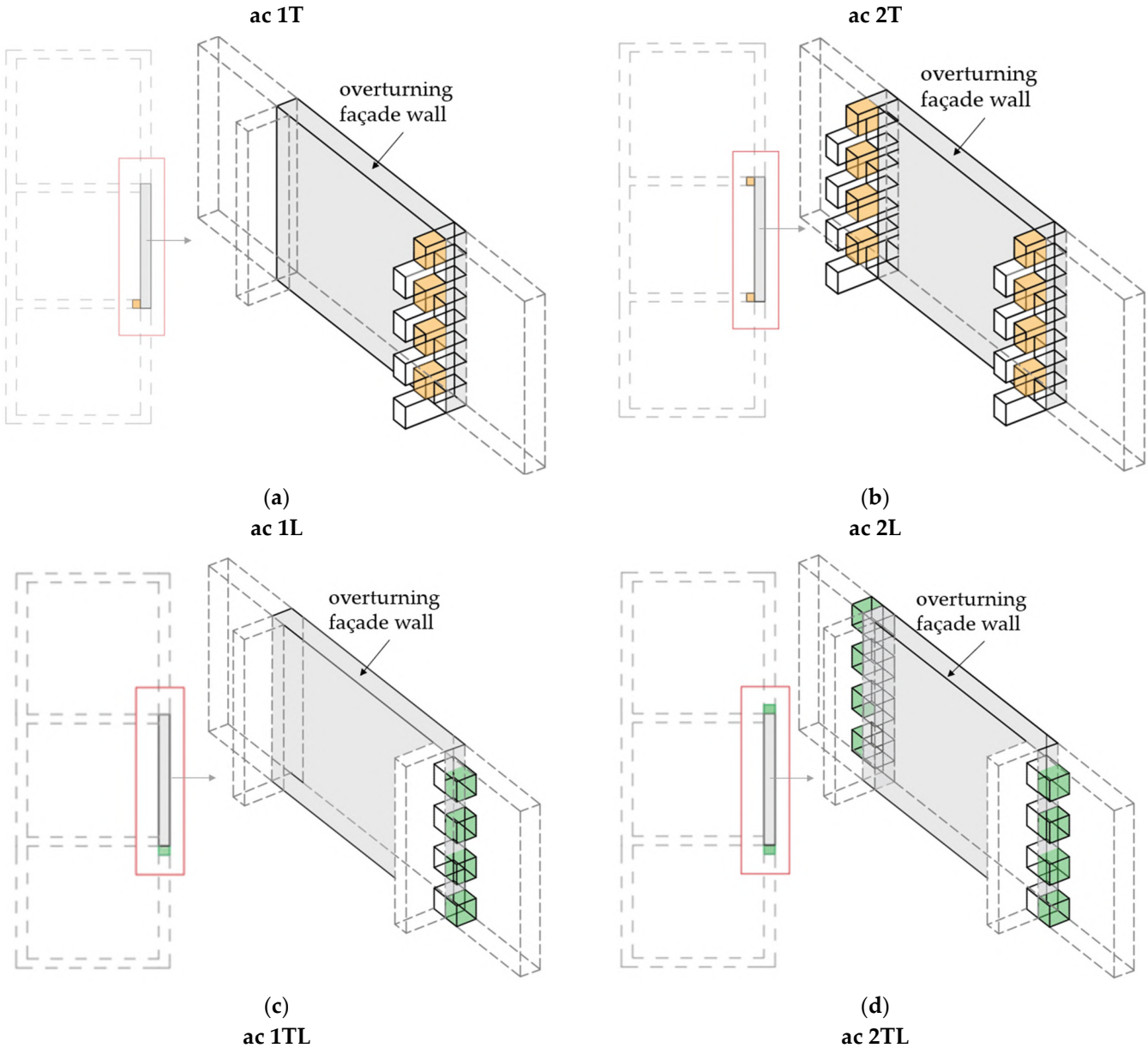

Figure 6. *Cont.*

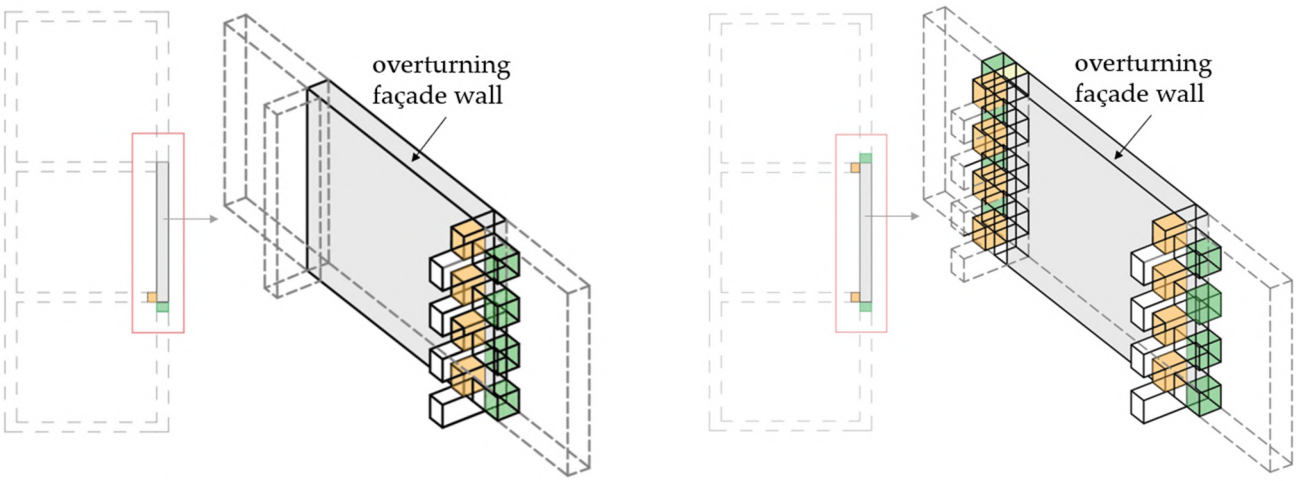

(**e**) (**f**)

Figure 6. Connection scenarios considered in this study: facade wall partially connected to the transverse walls on one side (**a**) and on both sides (**b**); façade wall partially connected to the lateral coplanar walls on one side (**c**) and on both sides (**d**); façade wall partially connected to both the transverse and lateral coplanar walls on one side (**e**) and on both sides (**f**).

3. Fragility Curves for URM Buildings Considering the *Aggregate Effect*

This section describes the proposed approach for deriving the fragility curves for URM buildings in aggregate that are susceptible to out-of-plane overturning mechanisms of their façade walls. The proposal introduces the *aggregate effect* to take into account interactions between adjacent buildings that may occur in case of buildings in aggregate configuration [5,38].

The proposed approach, similarly to that developed by the authors in their previous works [45,47] and referring to isolated buildings, follows the multi-step procedure outlined in Figure 7. Each step is described in detail, providing specific evidence of the contribution of the *aggregate effect*.

- Step 0 consists of defining the building typologies representative of the area of study, on the basis of similar structural–typological features and the age of construction, as defined within the Italian DPC-ReLUIS CARTIS Project [51–53]. For each identified building typology, this step is also devoted to collect additional data specifically concerning the type of connection between S.U.s.
- Step 1 consists of identifying, for each building typology, subsets of buildings characterized by the same type of the most probable out-of-plane mechanism [50] and the same number of floors. For this purpose, each sample S.U. of the area under study is analyzed to define the corresponding most probable out-of-plane mechanism as proposed in [54]. Then, the building typologies defined in the previous step are subdivided in subsets of buildings with the same most probable out-of-plane mechanism and the same number of floors, called building categories.

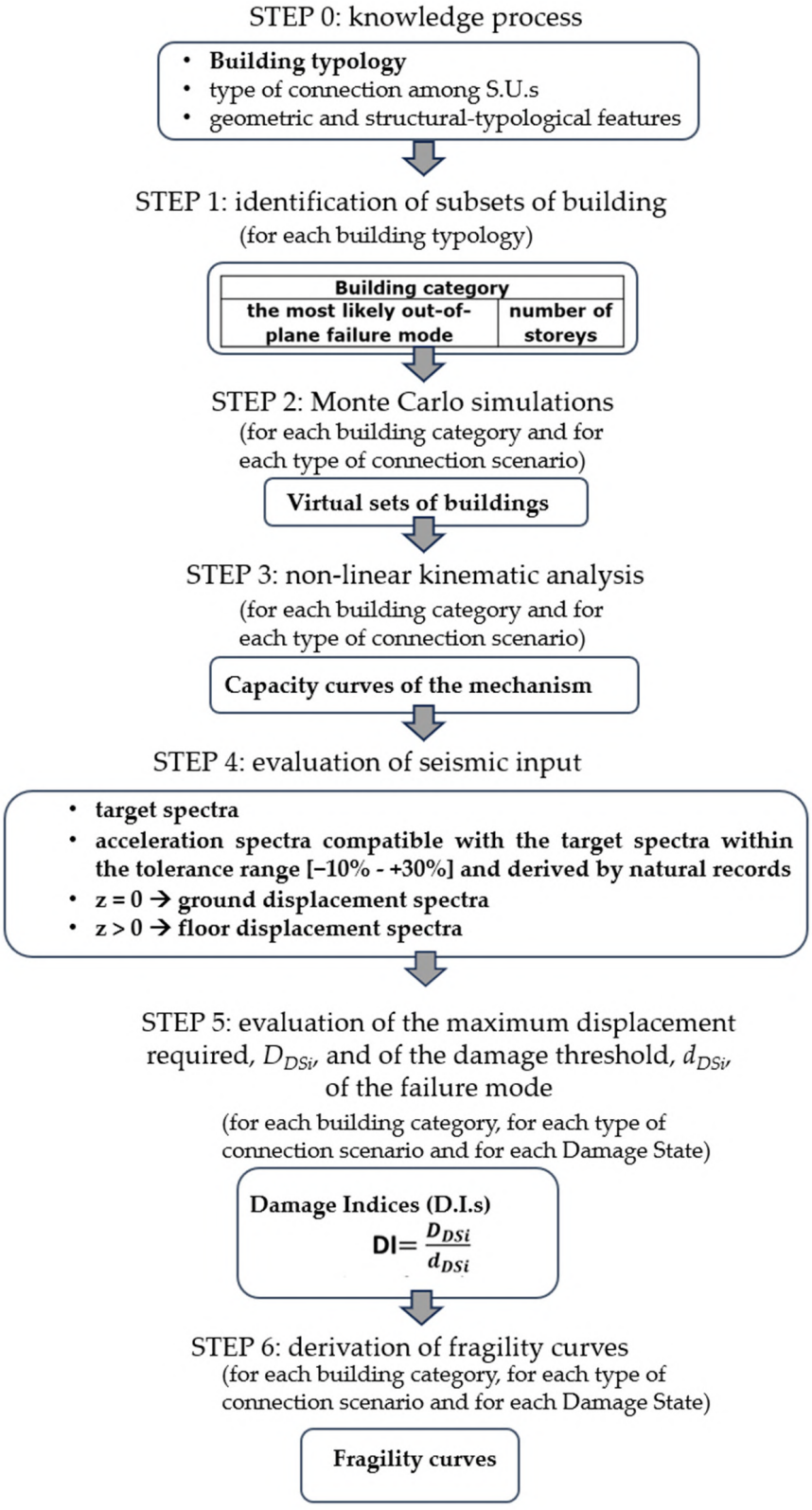

Figure 7. Workflow of the proposed approach.

- Step 2 consists of generating, for each building category, a set of 3000 virtual buildings through Monte Carlo simulations. The virtual buildings are generated by varying the following parameters of the facade walls: wall thickness, inter-story height, percentage of holes, and masonry compressive strength. Each parameter is varied by assuming

a lognormal distribution, commonly used to describe variables that can take on any value greater than or equal to zero [55,56]. The steps goes on with the generation of the height and the overlap length of the semi-blocks (h_{block} and $L_{block,overlap}$) to be associated with the 3000 virtual buildings. Since there is a lack of sample data on the geometric characteristics of semi-blocks, we opt for a uniform distribution to generate these dimensions. This approach aims to prevent any bias in the results. The resulting values of height and overlap length are then linked to each virtual building based on the type of connection scenarios among the S.U.s, as depicted in Figure 6. The following must be noted:

- In case of the connection scenarios "ac 1T", "ac 2T", "ac 1TL", and "ac 2TL", i.e., in case of connection of the façade wall with the transverse walls, both h_{block} and $L_{block,overlap}$ are associated with each virtual building;
- In case of the connections scenarios "ac 1L" and "ac 2L", i.e., in case of connection of the façade with the coplanar walls, only the h_{block} is associated with each building, since, in this case, the $L_{block,overlap}$ is coincident with the thickness of the adjacent coplanar walls.

- Step 3 is devoted to carrying out a nonlinear kinematic analysis of each virtual building belonging to each building category and evaluating the capacity curve of the corresponding mechanism in terms of spectral acceleration (a) vs. spectral displacement (d). In particular, the nonlinear kinematic analysis of the façade wall portion involved in the failure mode is conducted based on the following hypotheses:
  - There are rigid blocks, zero masonry tensile strength [50,57], and limited masonry compressive strength [58];
  - There is a consideration not only of the weight of the portion of wall involved in the failure mode, the corresponding horizontal seismic force, and any forces arising from loads transmitted from floors, vaults, and roofs, but also the friction force (F) due to the *aggregate effect* defined in the previous Section 2. It is important to note that, unlike the other acting forces, the resultant F is not constant during the evolution of the mechanism since it progressively reduces due to the gradual loss of the overlap between the blocks [59] (see Figure 8).

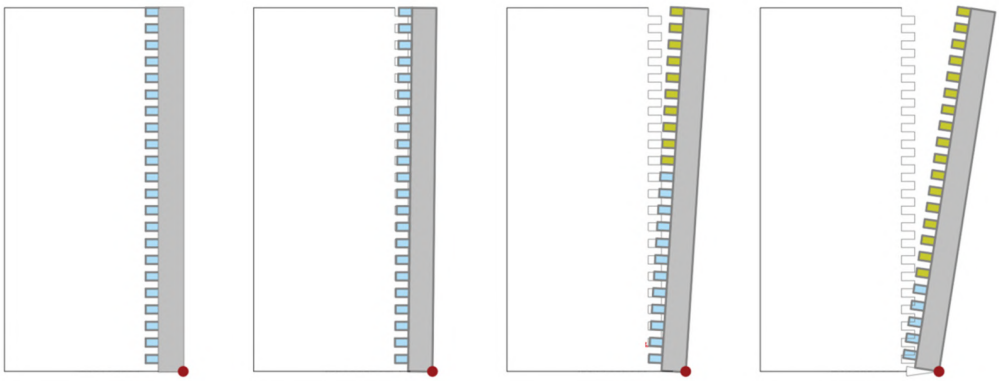

Figure 8. Evolution of the connection loss between the façade wall and the transversal wall during the progression/evolution of the overturning mechanism (interconnected semi-blocks are depicted in cyan until there is overlap between them, after which they are depicted in yellow).

In order to evaluate the value of the friction force during the mechanism, it is necessary to determine its ultimate value, F_u, at the loss of equilibrium. F_u is evaluated iteratively by varying, at each iteration, the value of the acting frictional forces, as described in [59].

Once the value of F_u has been defined, the force F_b during the evolution of the mechanism is evaluated with Equation (1) by replacing n with r, where r represents the number of rows of overlapping blocks, defined as

$$r = n - 2i \quad (4)$$

In Equation (4), $2i$ is the number of block rows that lose contact during the evolution of the kinematics [59], which is equal to zero at the activation of the mechanism.

The contribution of the friction force due to overloads, F_q, on the other hand, disappears as soon as the contact between the blocks at the top of each story is lost.

- Step 4 is finalized to evaluate the seismic input of the site in terms of the compatible displacement spectra derived by natural records. For this purpose, the following occurs:
  - Reference spectra of the site under consideration (target spectra) are selected by considering eight different return periods;
  - The "disaggregation" technique is used to identify natural records with similar characteristics, in terms of magnitude and distance, to those expected at the site [60,61];
  - Records whose average acceleration spectra are compatible with the target spectra within a pre-defined tolerance range [−10%–+30%] [62] are combined;
  - The acceleration spectra corresponding to the 16th and 84th percentiles are evaluated for each defined combination of records;
  - From the obtained acceleration spectra, the corresponding spectra in terms of ground and floor displacements are derived.
- Step 5 is finalized for calculating the variable Damage Index (D.I.), which represents the degree of the Damage State (D.S.) achieved. This variable is determined for two distinct D.S.s:
  - The first, called DS1 and corresponding to the activation of the mechanism;
  - The second, called DS2 and corresponding to the collapse of the portion of the façade affected by the mechanism.

  In particular, Step 5 is finalized to calculate the variable Damage Index (D.I.) of each virtual building. This variable represents the degree of the Damage State (D.S.) achieved and is evaluated as the ratio between the maximum required displacement of the D_{DSi} (demand) mechanism and the damage threshold of the d_{DSi} (capacity) mechanism.
  The demand is determined by using the displacement spectra obtained in Step 4 and by applying the capacity spectrum method [63]. Specifically, ground displacement spectra are used if the considered mechanism occurs at z = 0 [50]; conversely, floor displacement spectra [64] are used if the considered mechanism occurs at z > 0 [50].
  The capacity in terms of the damage threshold, d_{DSi}, on the other hand, is derived from the capacity curves derived in Step 3. The damage threshold corresponding to DS1 is identified by the spectral displacement (d_y) at the intersection between the capacity curve and a linear branch representing the elastic behavior of the façade wall before the activation of the mechanism. Conversely, the damage threshold of DS2 corresponds to the collapse defined by a damage threshold of 0.40 d_0, where d_0 is the spectral displacement corresponding to the point where the spectral acceleration (a) is zero [50,65,66] (see Figure 9).

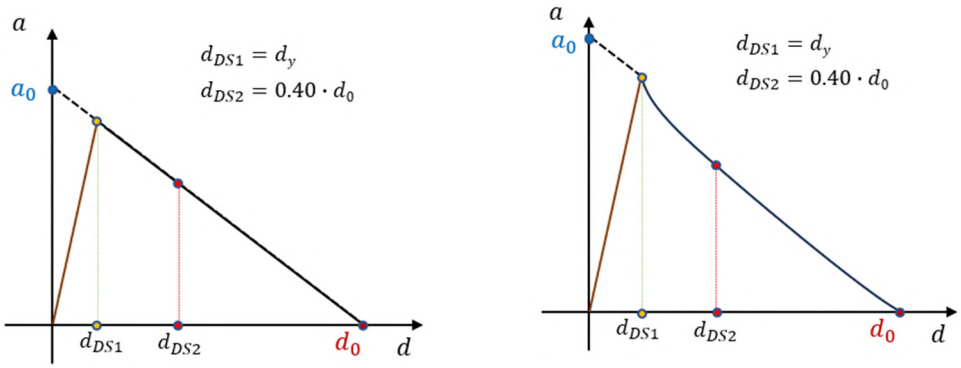

Figure 9. Damage thresholds derived with (**a**) no *aggregate effect*; (**b**) presence of *aggregate effect* and defined on the mechanism capacity curve (black color line) considering a linear branch (brown color line) representing the elastic behavior of the facade wall before mechanism activation.

- Step 6 concerns the evaluation of the fragility curves for the two D.S.s for each building category. Using the Peak Ground Acceleration (PGA) as the intensity measure, the fragility curves are assessed by considering a lognormal distribution for the D.I.s [35,55,67], with the following:
  - The mean values obtained through a linear regression of the natural logarithm of the DIs versus the natural logarithm of the PGA [68];
  - The derived total dispersion incorporating both the model variability [69] and the record-to-record variability. The latter is estimated using the 84th and the 16th percentiles of the selected spectra [45,70].

Steps 5 and 6 are carried out for each set of the virtual buildings corresponding to the six possible connection scenarios. In this regard, it is evident that the connection scenario could significantly influence the seismic vulnerability assessment of URM buildings in an aggregate configuration. Nevertheless, investigations aimed at defining the connection scenario could be challenging to conduct, expensive, and time-consuming. Therefore, in the preliminary phase of analysis, all possible connection scenarios can be considered to identify the most hazardous conditions.

4. Case Study

The urban area considered as a case study in this paper is the historical center of Sora (Figure 10), a municipality of the Lazio region located in Central Italy. The authors investigated this center as part of the CARTIS research project, a project funded by the Italian Civil Protection Department and aimed at characterizing ordinary Italian buildings [51,52]. The center consists mainly of two URM building typologies, denoted here with the labels "BT 1" and "BT 2". The "BT 1" typology is characterized by two- and three-story buildings, built before 1860 in uneven masonry with rough stones (Figure 11a), and presents mainly wooden slabs (Figure 11b). The "BT 2" typology is characterized by S.U.s built from 1861 to 1919 in regular masonry with square stones and has hollow-core concrete slabs. Based on research conducted by the authors within the CARTIS database [47,48], the two typologies are notably prevalent in central Italy, particularly in the municipalities of the central Apennines. Therefore, they can be considered representative of the typical buildings found in the historic centers of these areas. Figure 12 shows the typical buildings representative of the two typologies. For a more detailed characterization, refer to [45].

Figure 10. Map of the historical center of Sora.

(**a**) (**b**)

Figure 11. (**a**) Masonry typology characterizing the building typology "BT 1"; (**b**) slab in wood for a building belonging to the building typology "BT 1".

(**a**) (**b**)

Figure 12. Examples of buildings in aggregate configuration belonging to the (**a**) "BT 1" typology and (**b**) "BT 2" typology.

4.1. Application of the Proposed Approach

The knowledge process (Step 0) did not provide enough information to determine the specific types of connections between buildings. Therefore, for the application of the proposed approach, reference has been made to the presence of all possible configurations, including both the isolated one and the six possible connection scenarios for the aggregate configuration.

For each of the two building typologies defined within Step 0, the application of the second step led to the division of each typology into ten building categories as shown in Table 1. This classification includes the following:

- One category for global simple overturning;
- Three categories for simple partial overturning;
- Two categories for global overturning along the openings;
- Two categories for horizontal bending;
- Two categories for vertical bending.

Table 1. Building categories into which the building typologies characterizing the historic center of Sora have been divided.

Building Category	The Most Likely Out-of-Plane Failure Mode	Number of Stories
1	Global simple overturning	3
2	Simple partial overturning of the 2nd story	2
3	Simple partial overturning of the 3rd story	3
4	Simple partial overturning of the 2nd and the 3rd story	3
5	Global overturning along the openings	2
6	Global overturning along the openings	3
7	Horizontal bending	2
8	Horizontal bending	3
9	Vertical bending	2
10	Vertical bending	3

Next, for each of the categories characterized by the overturning mechanisms (from 1 to 6), 3000 virtual buildings were generated using the Monte Carlo method. The generations were carried out by varying the wall thickness, the inter-story height, the number of holes in the façade, and the masonry compressive strength [46]. In this regard, it is assumed that the values of the above parameters follow a lognormal distribution [55]. Specifically, the geometrical parameters of each building story and the masonry compressive strength values were generated using the mean and standard deviation values listed in Table 2. In particular, the means and the standard deviations of the wall thickness, inter-story height, and holes in the façade were obtained by calculating the means and the standard deviations of the corresponding real data for each story belonging to the sample buildings of the case study. To this end, the sample data were derived by an in-depth survey conducted in [54,71]. The values of the mean and the standard deviation of the masonry compressive strength were, instead, set equal to those characterizing the masonry typologies of the case study buildings recommended in [55] (the uneven masonry with rough stones and the regular masonry with square stones, respectively, for "BT 1" and "BT 2").

In addition, for the analysis of the walls in aggregate configuration, the corresponding dimensions of the interconnecting semi-blocks were associated with each generated virtual building. They were simulated by the Monte Carlo method and the dimensions were assumed to vary with a uniform distribution within a range specific to the examined building typology (see Table 3).

Table 2. Values of mean and standard deviation used to generate the parameters of the virtual sets of buildings for each building category.

Parameter	Building Floor Number	"BT 1"		"BT 2"	
		Mean	Standard Deviation	Mean	Standard Deviation
wall thickness [m]	1st	−0.35	0.17	−0.41	0.11
	2nd	−0.44	0.20	−0.51	0.08
	3rd	− 0.48	0.20	−0.60	0.08
inter-story height [m]	1st	1.08	0.21	1.16	0.16
	2nd	1.07	0.13	1.10	0.06
	3rd	1.01	0.26	1.07	0.10
holes in façade [-]	1st	−0.62	0.17	−0.52	0.11
	2nd	−0.19	0.09	−0.20	0.11
	3rd	0.26	0.12	−0.31	0.13
masonry compressive strength [N/cm^2]	-	4.94	0.29	5.25	0.27

Table 3. Ranges used to generate the height (h_{block}) and the overlap length ($L_{block,overlap}$) of the interconnecting semi-blocks.

Building Typology	1st Story		2nd Story		3rd Story	
	h_{block} [m]	$L_{block,overlap}$ [m]	h_{block} [m]	$L_{block,overlap}$ [m]	h_{block} [m]	$L_{block,overlap}$ [m]
BT 1	0.30–0.40	0.20–0.25	0.20–0.30	0.11–0.20	0.10–0.20	0.05–0.11
BT 2	0.09–0.15	0.15–0.20	0.09–0.15	0.15–0.20	0.09–0.15	0.15–0.20

It is important to note that, due to a lack of reliable information on the size of the blocks used in the buildings of this case study, the ranges for varying the semi-block dimensions were chosen by considering values derived from expertise judgments based on the common properties that characterize local URMs.

For the "BT 1" typology, the blocks were varied within different ranges depending on the building's story and in order to account for the following considerations:

- The use of larger square blocks as cornerstones on the ground story, which reflects local tradition [72] (see Figure 13);
- The gradual reduction in the block size used for the wall construction, from the ground story to the upper ones, as it is characteristic of this typology.

For the "BT 2" typology, the dimensions of the blocks varied within the same range for all the stories of the buildings.

For each building category, the capacity curve of each generated building was evaluated, within Step 3, by performing a nonlinear kinematic analysis on the wall part involved in the mechanism. Note that, for each category, seven sets of curves were obtained: the curves were derived by considering both the wall in isolated configuration and that in an aggregate configuration, according to the six different connection scenarios detailed in Section 2 (Figure 3). Clearly, the friction force is considered only in the case of a building in aggregate configuration and not in the case of an isolated building (in the case of an isolated building, friction forces are not considered).

Figure 13. Square blocks at the corner of the ground story.

Step 4 was performed to select the combinations of the acceleration spectra compatible with the target spectra of the area under the study, in compliance with [62]. In particular, the target spectra were defined for eight return periods, ranging from 30 to 975 years, considering that the area where the case study is located is characterized by a flat topographic surface, corresponding to a topographical category (T1), and by a subsoil category (D) [45]. The compatible spectra combinations, instead, were derived through the REXEL v.3.5 software [73] from the natural records included in the ITACA Database [74]. For each of the spectra combinations, the average and the 84th and the 16th percentile spectra of the selected records were derived. The obtained acceleration spectra were converted into ground displacement spectra (for mechanisms triggering at the base of the building's ground story) or into floor displacement spectra (for mechanisms triggering at higher floors) [45,46].

Having obtained the capacity curves and the spectra in terms of displacement, the damage thresholds, the maximum demands required for the mechanisms, and the related DIs were then determined according to Step 5, for each building category and for both DSs considered within the approach. Step 5 was carried out for both isolated and aggregated wall configurations in order to define the corresponding fragility curves, according to Step 6.

The most relevant results obtained in terms of capacity and fragility curves are presented and discussed in Sections 4.1 and 4.2, respectively.

4.2. Results and Discussion

Figures 14 and 15 present the envelopes of the capacity curves obtained for the building category of the three-story buildings susceptible to the global overturning mechanism and belonging to the typology "BT 2". The curves are expressed in terms of the spectral acceleration (a) vs. the spectral displacement (d). The envelope reported in Figure 14 refers to the case of the wall in isolated configuration; the envelopes reported in Figure 15 correspond to the six different aggregate configuration scenarios considered in this study.

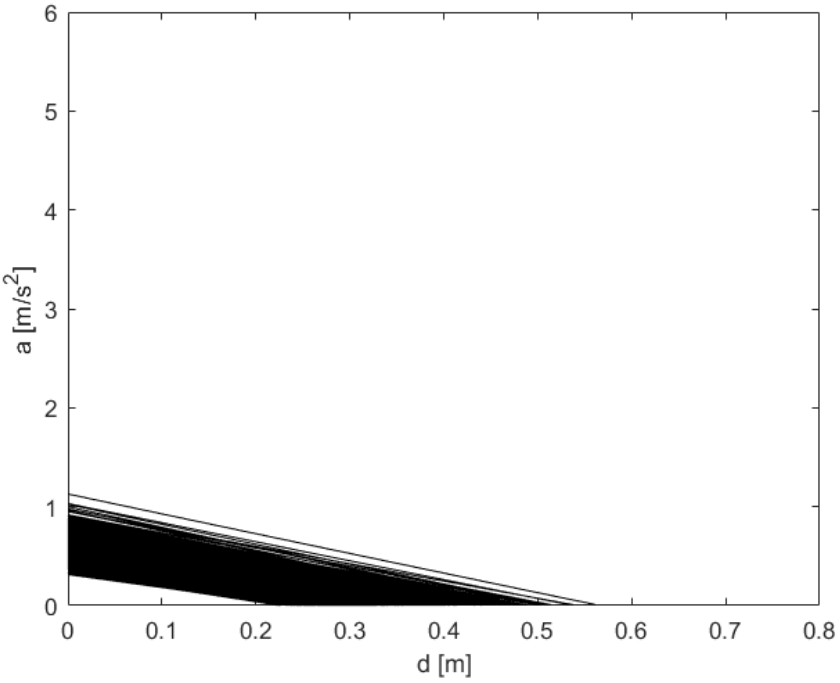

Figure 14. Capacity curves for the building category of 3-story buildings prone to the global overturning mechanism, part of the typology "BT 2", derived for the walls in isolated configuration.

The curves related to the isolated configuration have a linear trend. The curves corresponding to the aggregate configuration have a linear trend as long as the forces acting on the wall are constant; then, as soon as the overlapping between the interconnecting blocks begins to be lost, the curves decrease with a nonlinear trend.

Comparing the envelopes of the capacity curves shown in Figures 14 and 15, it is clear that both the spectral acceleration corresponding to the activation of the mechanism (i.e., the first point of the capacity curves) and the ultimate spectral displacement of the mechanism (i.e., the last point of the capacity curves) depend on the type of configuration and on the type of interconnection scenarios. In particular, the spectral accelerations corresponding to the activation increase from values in the range [0.3–1.2] m/s^2, for the wall in isolated configuration, to values in the following ranges:

- A range of [0.8–1.8] m/s^2 for walls partially connected to the transverse walls of the adjacent S.U. on one side (Figure 15a);
- A range of [1.2–3.0] m/s^2 for walls partially connected to the transverse walls of the adjacent S.U. on both sides (Figure 15b);
- A range of [0.8–2.2] m/s^2 for walls partially connected to the lateral walls of the adjacent S.U. on one side (Figure 15c);
- A range of [1.2–3.6] m/s^2 for walls partially connected to the lateral walls of the adjacent S.U. on both sides (Figure 15d);
- A range of [1.2–3.2] m/s^2 for walls partially connected to the transverse and lateral walls of the adjacent S.U. on one side (Figure 15e);
- A range of [2.0–5.8] m/s^2 for walls partially connected to the transverse and lateral walls of the adjacent S.U. on one side (Figure 15f).

The last point of the capacity curves shifts to the right in the presence of the aggregate configurations, moving from values varying in the range of 0.22–0.56 m to values in the range of 0.4–0.77 m in the case of walls partially connected to the transverse and lateral walls on both sides.

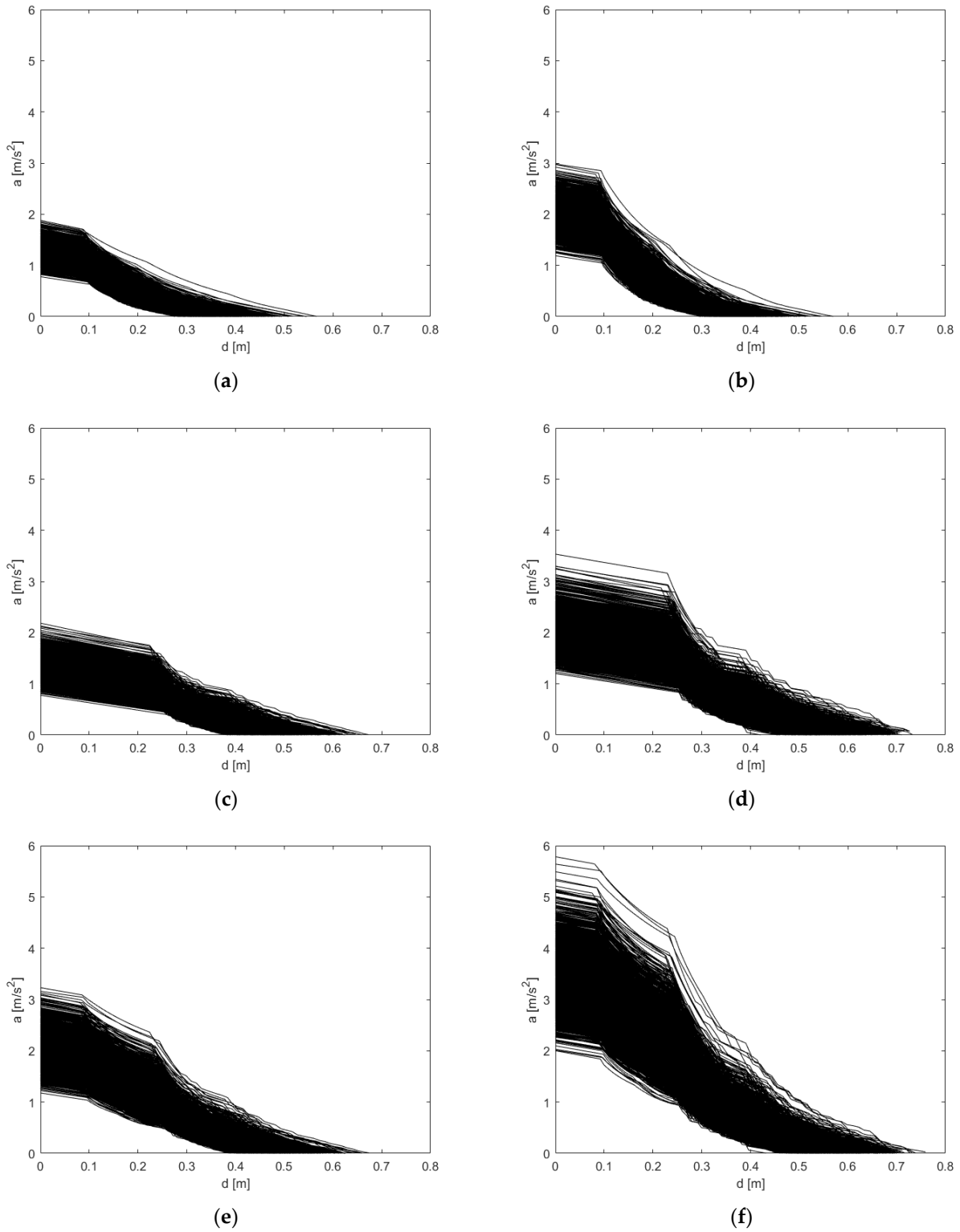

Figure 15. Capacity curves for the building category of 3 story-buildings susceptible to the global overturning, part of the typology "BT 2", derived for the case of (**a**) façade walls partially connected to the transverse walls of the adjacent S.U. on one side; (**b**) façade walls partially connected to the transverse walls of the adjacent S.U. on both sides; (**c**) façade walls partially connected to the lateral walls of the adjacent S.U. on one side; (**d**) façade walls partially connected to the lateral walls of the adjacent S.U. on both side (**e**) façade walls partially connected to the transverse and lateral walls of the adjacent S.U. on one side; (**f**) façade walls partially connected to the transverse and lateral walls of the adjacent S.U. on one side.

The fragility curves obtained for the three-story building categories, which are part of the two building typologies of this case study, are reported in Figures 16–22.

In each figure, the curves in gray are related to DS1 and those in blue correspond to DS2. In particular, the following can be noted:

- The curves "DS1 ic" and "DS2 ic" represent the ones related to the façade wall in isolated configuration, for DS1 and DS2, respectively;
- The curves "DS1 ac 1T" and "DS2 ac 1T" are the ones obtained considering the façade wall in the connection scenario "ac 1T" for DS1 and DS2, respectively;
- The curves "DS1 ac 2T" and "DS2 ac 2T" represent the ones obtained considering the façade wall in the connection scenario "ac 2T" for DS1 and DS2, respectively;
- The curves "DS1 ac 1L" and "DS2 ac 1L" represent the ones obtained considering the façade wall in the connection scenario "ac 1L" for DS1 and DS2, respectively;
- The curves "DS1 ac 2L" and "DS2 ac 2L" represent the ones obtained considering the façade wall in the connection scenario "ac 2L" for DS1 and DS2, respectively;
- The curves "DS1 ac 1TL" and "DS2 ac 1TL" represent the ones obtained considering the façade wall in the connection scenario "ac 1TL" for DS1 and DS2, respectively;
- The curves "DS1 ac 2TL" and "DS2 ac 2TL" represent the ones obtained considering the façade wall in the connection scenario "ac 2TL" for DS1 and DS2, respectively.

Figures 16 and 17 show the fragility curves obtained for the building category of three-story buildings susceptible to the global overturning mechanism, part of the "BT 1" and "BT 2" building typologies, respectively.

Building typology: "BT 1"
Building category: 3-story buildings susceptible to the global overturning

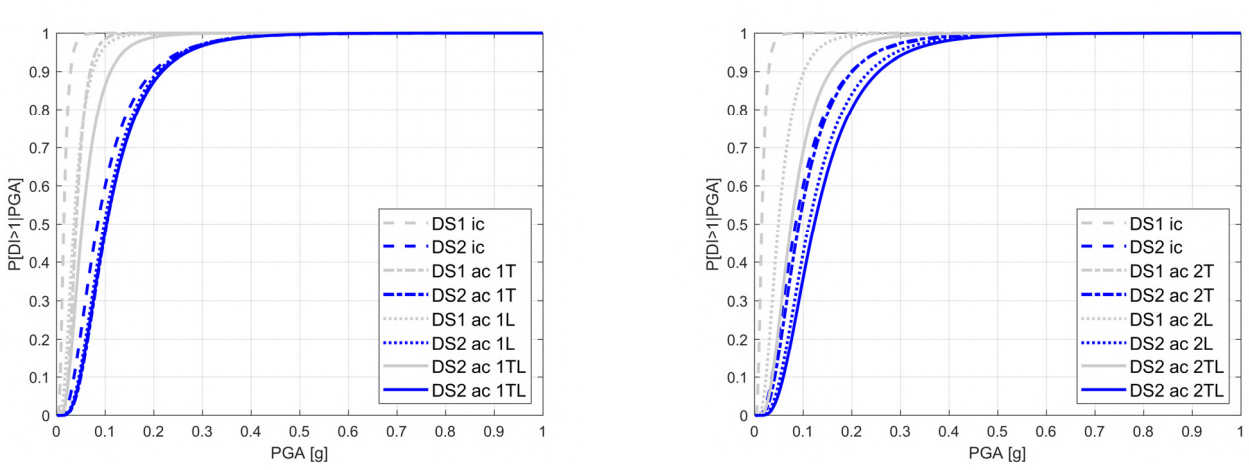

(**a**) (**b**)

Figure 16. Overlap between the fragility curves obtained for the case of walls in isolated configuration (dashed line) and those obtained for walls in aggregate configuration with transverse connection (stretched-dot line), with lateral connection (dotted line), and with the co-presence of transverse and lateral connection (solid line) (**a**) on one side only and (**b**) on both sides.

Building typoogy: "BT 2"
Building category: 3-story buildings susceptible to global overturning

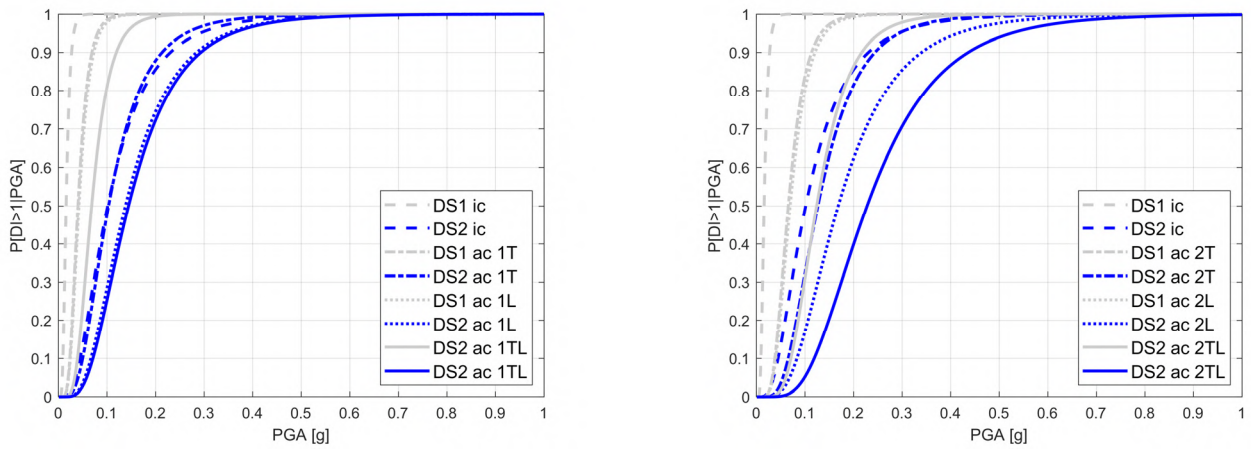

(**a**) (**b**)

Figure 17. Overlap between the fragility curves obtained for the case of walls in isolated configuration (dashed line) and those obtained for walls in aggregate configuration with transverse connection (stretched-dot line), with lateral connection (dotted line), and with the co-presence of transverse and lateral connection (solid line) (**a**) on one side only and (**b**) on both sides.

The fragility curves of the three-story building category susceptible to global overturning along the openings, belonging to the "BT 1" and "BT 2" building typologies, respectively, are shown in Figure 18.

Building typoogy: "BT 1" **Building typology: "BT 2"**
Building category: 3-story buildings susceptible to the global overturning along the openings

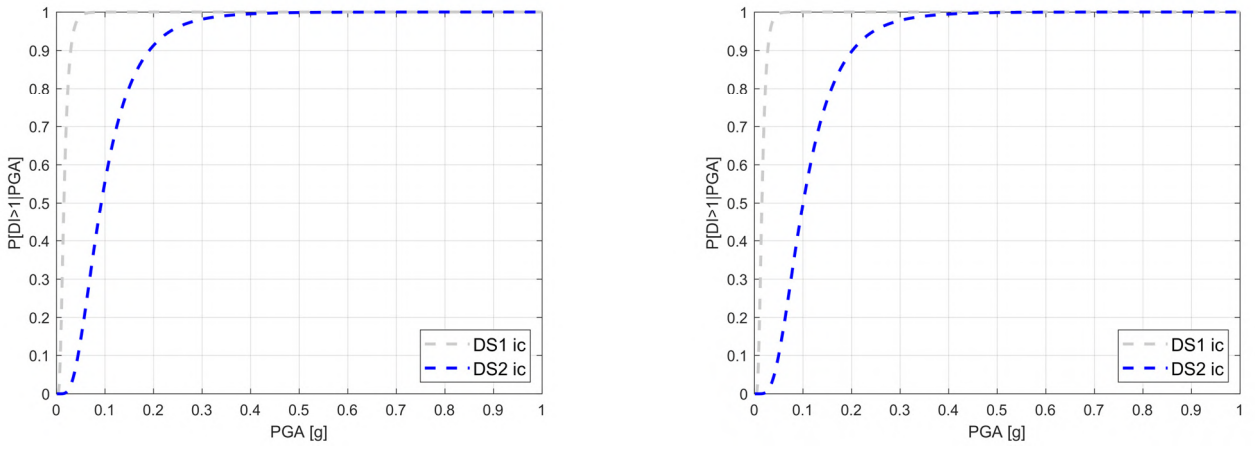

(**a**) (**b**)

Figure 18. Fragility curves for the building category of 3-story buildings susceptible to global overturning along the openings, part of (**a**) the typologies "BT 1" and (**b**) "BT 2".

Figures 19 and 20 present the fragility curves derived for the building category of three-story buildings susceptible to the partial overturning mechanism of the third story, part of the "BT 1" and "BT 2" building typologies, respectively.

Building typology: "BT 1"
Building category: 3-story buildings susceptible to the partial overturning of the 3rd story

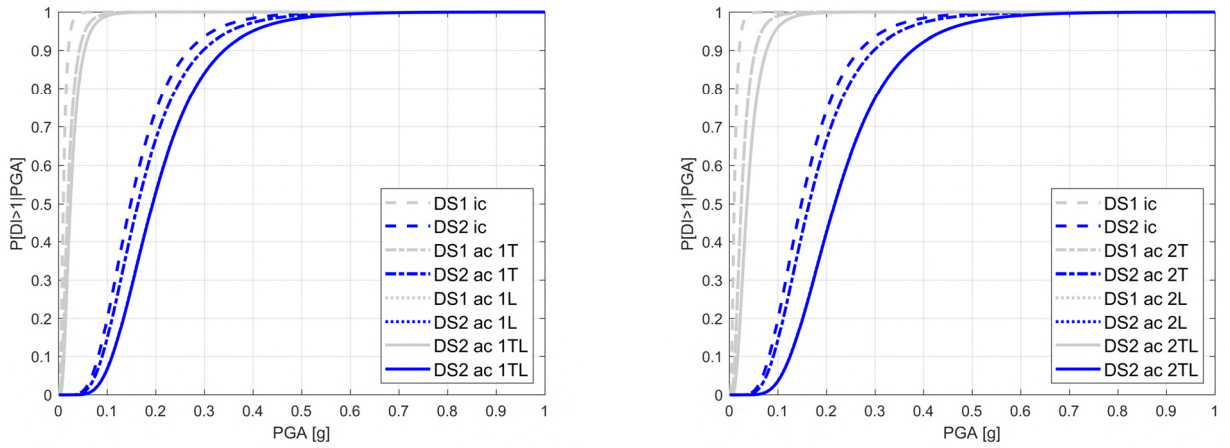

(**a**) (**b**)

Figure 19. Overlap between the fragility curves obtained for the case of walls in isolated configuration (dashed line) and those obtained for walls in aggregate configuration with transverse connection (stretched-dot line), with lateral connection (dotted line), and with the co-presence of transverse and lateral connection (solid line) (**a**) on one side only and (**b**) on both sides.

Building typology: "BT 2"
Building category: 3-story buildings susceptible to the partial overturning of the 3rd story

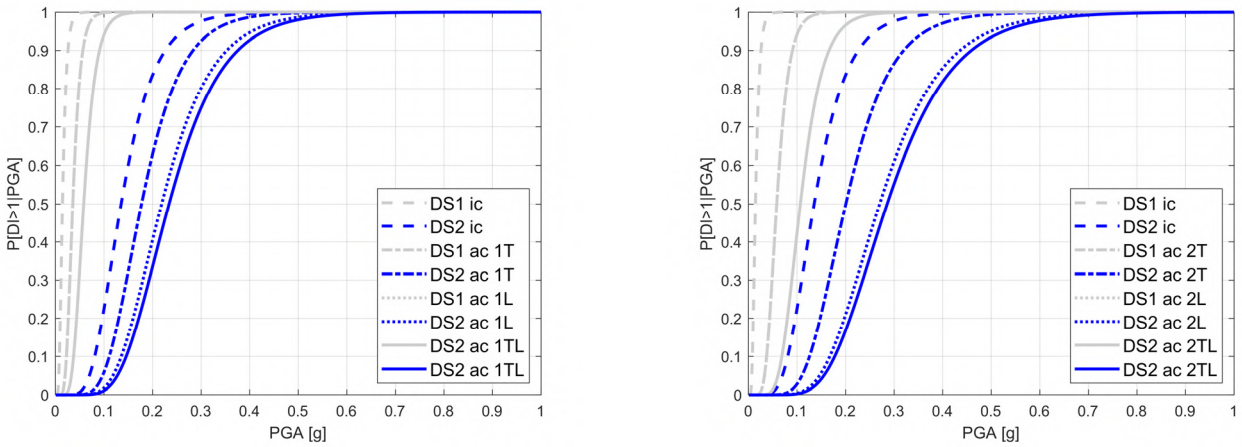

(**a**) (**b**)

Figure 20. Overlap between the fragility curves obtained for the case of walls in isolated configuration (dashed line) and those obtained for walls in aggregate configuration with transverse connection (stretched-dot line), with lateral connection (dotted line), and with the co-presence of transverse and lateral connection (solid line) (**a**) on one side only and (**b**) on both sides.

Figures 21 and 22 present the fragility curves of the building category of three-story buildings susceptible to the partial overturning mechanism of the second and third stories, part of the "BT 1" and "BT 2" building typologies, respectively.

Building typology: "BT 1"
Building category: 3-story buildings susceptible to the partial overturning of the 2nd and of the 3rd story

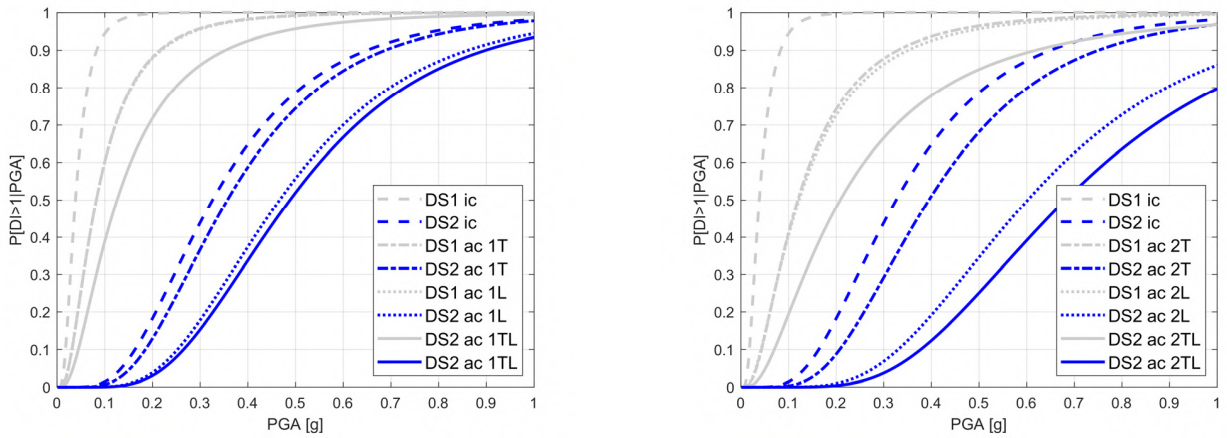

(**a**) (**b**)

Figure 21. Overlap between the fragility curves obtained for the case of walls in isolated configuration (dashed line) and those obtained for walls in aggregate configuration with transverse connection (stretched-dot line), with lateral connection (dotted line), and with the co-presence of transverse and lateral connection (solid line) (**a**) on one side only and (**b**) on both sides.

Building typology: "BT 2"
Building category: 3-story buildings susceptible to the partial overturning of the 2nd and of the 3rd story

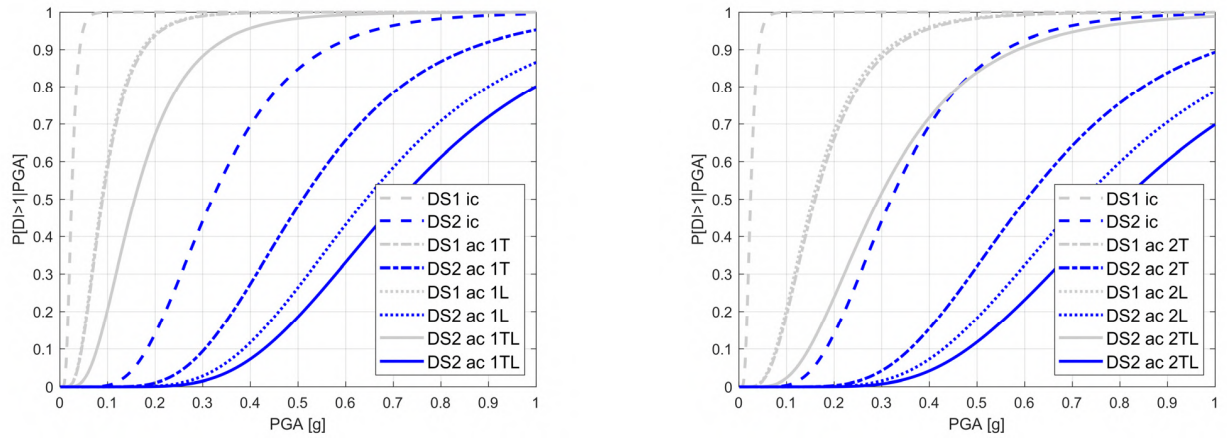

(**a**) (**b**)

Figure 22. Overlap between the fragility curves obtained for the case of walls in isolated configuration (dashed line) and those obtained for walls in aggregate configuration with transverse connection (stretched-dot line), with lateral connection (dotted line), and with the co-presence of transverse and lateral connection (solid line) (**a**) on one side only and (**b**) on both sides.

The comparison of the fragility curves of buildings in isolated configuration with those of buildings in aggregate configuration shown in Figures 16–22 reveals that the *aggregate effect* has a beneficial influence on the seismic behavior of the buildings: in the case of aggregate configuration, the fragility of the overturning mechanisms decreases for both DS1 and DS2.

By observing the curves, it is noticeable that, for the same building category, the curves related to the same DS but corresponding to a different configuration (isolated and in aggregate) related to the "BT 1" building typology are closer to each other than those related to "BT 2". In particular, for the same building category, DS, and connection type,

buildings belonging to "BT 2" are characterized by lower fragility; i.e., the same PGA corresponds a lower probability of reaching or exceeding the DS.

To highlight the influence of the *aggregate effect*, the PGA value was evaluated for both isolated and aggregate configurations, considering the following factors: Limit State DS2; probability of exceeding 50%; overturning of the third floor only or overturning of the second and third floors; and units connected to adjacent ones on one side only or on two sides. By comparing the obtained values, it is possible to observe the following trends (see Figure 19):

One-sided connection:

- In the case of overturning of the third floor, the introduction of the *aggregate effect* leads to an increase in PGA of 47% for "BT 1" and 87% for "BT 2".
- In the case of overturning of the second and third floors, it leads to an increase in PGA of 54% for "BT 1" and 174% for "BT 2".

Two-sided connection:

- For overturning of the third floor, the *aggregate effect* leads to an increase in PGA of 12% for "BT 1" and 25% for "BT 2".
- For overturning of the second and third floors, the *aggregate effect* leads to an increase in PGA of 20% for "BT 1" and 48% for "BT 2".

These results demonstrate that the influence of the *aggregate effect* depends on both the connection scenario and the building typologies. In particular, the *aggregate effect* is limited for buildings of "BT 1" but is relevant for buildings of "BT 2". The limited influence of the aggregate configuration for buildings of the "BT 1" typology results from the presence, in such buildings, of small interconnecting blocks on the upper floors. These blocks rapidly lose contact with each other as the tilting progresses, and the beneficial effect of the friction quickly disappears. In contrast, buildings of the "BT 2" typology have larger interconnecting blocks on the upper floors. These larger blocks maintain contact with the adjacent walls longer during overturning, resulting in a significant reduction in vulnerability for the "BT 2" typology in aggregate configurations compared to that in isolated ones. Further, it is also evident how the lateral connection is more effective than the transverse one in reducing the seismic vulnerability. Indeed, the capacity curves of Figure 15 show that sliding between blocks starts at higher levels of PGA, due to the fact that the contact surface between blocks is larger than in the case of transverse connection.

5. Conclusions

The present research work presents an approach specifically developed for the seismic vulnerability assessment of URM buildings in an aggregate configuration. Its main novelty with respect to existing methods is accounting for the potential interactions between adjacent buildings (*aggregate effect*) for the derivation of fragility curves. The latter in particular were derived by focusing attention on the out-of-plane mechanisms often affecting the façade walls of buildings in historic urban areas.

The approach operates in seven steps. It begins with defining the prevalent building typologies in the urban area, considering factors such as construction age, construction technique, and structural features. It then identifies how adjacent buildings are connected to each other at the intersection between the facade wall and the adjacent walls (Step 0). Then, for each building typology, it categorizes buildings with the same most probable out-of-plane failure mode (e.g., global simple overturning) and the same number of floors. This categorization creates subsets of buildings for each building typology, known as building categories (Step 1).

For each building category, it generates 3000 virtual buildings and their corresponding semi-blocks using a Monte Carlo simulations (Step 2).

Each generated building is analyzed using a nonlinear kinematic approach to obtain the capacity curve of its most probable mechanism. This analysis incorporates the *aggregate effect* and considers six different types of connection scenarios (Step 3).

Then, the seismic input, in terms of displacement spectra derived from natural records, is evaluated for eight different return periods (Step 4).

The approach proceeds with the calculation of the D.I.s to represent the severity of damage for two specific D.S.s: the first corresponding to the mechanism activating and the second corresponding to the wall collapsing (Step 5).

Finally, the approach evaluates, for the two considered D.S.s, the fragility curves of each building category and each connection scenario (Step 6).

This paper also illustrates and discusses an application of the proposed approach to the historical center of Sora, a medium-sized town of Central Italy. To critically analyze the obtained results, both the aggregate configuration, with all the possible connection scenarios, and the isolated configuration are considered. The obtained results pointed out that the level of seismic vulnerability of the analyzed buildings can be strongly affected by the beneficial influence of the *aggregate effect*, particularly depending on the configuration of the structural details characterizing the connections among adjacent facades (interlock). This suggests that one of the key aspects to consider, within the knowledge process, is the type of connection that characterizes the facade wall of S.U.s of the building aggregates. However, the potential lack of details on the geometrical characteristics of semi-blocks could represent a limitation during the implementation of the procedure. To overcome these limitations, the approach assumes a uniform distribution for these features.

The proposed approach is readily applicable to other urban areas; its application only requires knowledge of the characteristics of representative sample buildings in the area under study in order to be able to determine the prevailing building types, identify the types of connections between buildings and the most likely out-of-plane mechanisms, and evaluate the mean and standard deviation of the parameters needed to generate the virtual buildings. This information can be obtained from available databases or from archival documents and site surveys.

As a final consideration, it can be observed that the proposed approach represents a valuable tool for the large-scale vulnerability assessment of existing buildings in historical centers and the planning of a more environmentally friendly disaster prevention strategy. In particular, taking the *aggregate effect* into account can lead to the planning of a more cost-effective and targeted seismic mitigation plan for historic urban areas. Indeed, the results of the approach could be useful to identify the most vulnerable buildings of a specific area and, thus, to define the interventions finalized to safeguard the building heritage of the historical centers. For example, understanding the most vulnerable structural units (S.U.s) in an urban area in relation to a certain level of earthquake shaking can inform decisions regarding strengthening measures or retrofitting interventions. Furthermore, the information provided by the application of the approach can be used to evaluate the resilience of transportation networks of the urban area, helping to plan for potential disruptions caused by earthquakes.

The findings of this research work could have several future developments. First, the proposed approach could be refined to include the soil–foundation–structure interaction effect [75]. Additionally, the approach could be extended to other types of out-of-plane failure modes and in-plane mechanisms.

Author Contributions: Conceptualization, V.C., V.T., E.G. and M.I.; methodology, V.C., V.T. and E.G.; software, V.C.; formal analysis, V.C.; investigation, V.C. and V.T.; resources, V.C. and V.T.; data curation, V.C. and V.T.; writing—original draft preparation, V.C.; writing—review and editing, V.C., V.T., E.G. and M.I.; supervision, V.T., E.G. and M.I.; project administration, E.G. and M.I.; funding acquisition, M.I. All authors have read and agreed to the published version of the manuscript.

Funding: This research was funded by "Project DPC/ReLUIS 2022–2024—WP2. Inventory of existing structural and building typologies—CARTIS".

Data Availability Statement: The data presented in this study are available on request from the corresponding author.

Conflicts of Interest: The authors declare no conflicts of interest.

References

1. Formisano, A.; Ademovic, N. An Overview on Seismic Analysis of Masonry Building Aggregates. *Front. Built Environ.* **2022**, *8*, 966281. [CrossRef]
2. Battaglia, L.; Ferreira, T.M.; Lourenço, P.B. Seismic Fragility Assessment of Masonry Building Aggregates: A Case Study in the Old City Centre of Seixal, Portugal. *Earthq. Eng. Struct. Dyn.* **2021**, *50*, 1358–1377. [CrossRef]
3. Formisano, A. Theoretical and Numerical Seismic Analysis of Masonry Building Aggregates: Case Studies in San Pio Delle Camere (L'Aquila, Italy). *J. Earthq. Eng.* **2017**, *21*, 227–245. [CrossRef]
4. Moretić, A.; Chieffo, N.; Stepinac, M.; Lourenço, P.B. Vulnerability Assessment of Historical Building Aggregates in Zagreb: Implementation of a Macroseismic Approach. *Bull. Earthq. Eng.* **2023**, *21*, 2045–2065. [CrossRef]
5. Carocci, C.F. Small Centres Damaged by 2009 L'Aquila Earthquake: On Site Analyses of Historical Masonry Aggregates. *Bull. Earthq. Eng.* **2012**, *10*, 45–71. [CrossRef]
6. Baggio, C.; Bernardini, A.; Colozza, R.; Corazza, L.; Della Bella, M.; Di Pasquale, G.; Dolce, M.; Goretti, A.; Martinelli, A.; Orsini, G. *Field Manual for Post-Earthquake Damage and Safety Assessment and Short Term Countermeasures (AeDES)*; European Commission—Joint Research Centre—Institute for the Protection and Security of the Citizen: Luxembourg, 2007; p. 22868.
7. Ortolani, B.; Borghini, A.; Boschi, S.; del Monte, E.; Vignoli, A. Study of Vulnerability and Damage: The Case Study of Castelnuovo after L'Aquila Earthquake (Italy). In Proceedings of the 15th WCEE-World Conference of Earthquake Engineering, Lisbon, Portugal, 24–28 September 2012; pp. 1–10.
8. Bernardini, C.; Maio, R.; Boschi, S.; Ferreira, T.M.; Vicente, R.; Vignoli, A. The Seismic Performance-Based Assessment of a Masonry Building Enclosed in Aggregate in Faro (Portugal) by Means of a New Target Structural Unit Approach. *Eng. Struct.* **2019**, *191*, 386–400. [CrossRef]
9. Cima, V.; Bartolomeo, C.; Grande, E.; Imbimbo, M. Natural Fibers for Out-of-Plane Strengthening Interventions of Unreinforced Masonry Buildings in Aggregate Configuration. *Sustainability* **2022**, *14*, 9967. [CrossRef]
10. Bernardini, C.; Rui, M.; Boschi, S.; Ferreira, T.M.; Romeu, V.; Vignoli, A. The Seismic Vulnerability Assessment of a Stone Masonry Building Enclosed in Aggregate. In Proceedings of the 16th European Conference on Earthquake Engineering, Kyriazis Pitilakis, 18–21 June 2018.
11. Atalić, J.; Uroš, M.; Šavor Novak, M.; Demšić, M.; Nastev, M. The Mw5. 4 Zagreb (Croatia) Earthquake of March 22, 2020: Impacts and Response. *Bull. Earthq. Eng.* **2021**, *19*, 3461–3489. [CrossRef] [PubMed]
12. Vlachakis, G.; Vlachaki, E.; Lourenço, P.B. Learning from Failure: Damage and Failure of Masonry Structures, after the 2017 Lesvos Earthquake (Greece). *Eng Fail Anal* **2020**, *117*, 104803. [CrossRef]
13. Learning from Construction Failures Due to the 2009 L'Aquila, Italy, Earthquake. *J. Perform. Constr. Facil.* **2010**, *24*, 536–555. [CrossRef]
14. Sorrentino, L.; Cattari, S.; da Porto, F.; Magenes, G.; Penna, A. Seismic Behaviour of Ordinary Masonry Buildings during the 2016 Central Italy Earthquakes. *Bull. Earthq. Eng.* **2019**, *17*, 5583–5607. [CrossRef]
15. Parisi, F.; De Luca, F.; Petruzzelli, F.; De Risi, R.; Chioccarelli, E.; Iervolino, I. *Field Inspection after the May 20th and 29th 2012 Emilia-Romagna Earthquakes*; Rep., Italian Network of Earthquake Engineering University Laboratories. 2012. Available online: http://www.reluis.it (accessed on 29 December 2023).
16. Valluzzi, M.R.; Sbrogiò, L.; Saretta, Y.; Wenliuhan, H. Seismic Response of Masonry Buildings in Historical Centres Struck by the 2016 Central Italy Earthquake. Impact of Building Features on Damage Evaluation. *Int. J. Archit. Herit.* **2022**, *16*, 1859–1884. [CrossRef]
17. Modena, C.; Da Porto, F.; Valluzzi, M.R.; Guttuso, F.C.; Iannelli, P.; Rubino, C. Sustainable Approaches to the Assessment and Mitigation of Seismic Risk and of the Effects of Earthquake Induced Damages to Historic Urban Centers. In *Structural Analysis of Historical Constructions: Anamnesis, Diagnosis, Therapy, Controls*; CRC Press: Boca Raton, FL, USA, 2016; pp. 35–43.
18. Giuliani, F.; De Falco, A.; Cutini, V. Rethinking Earthquake-Related Vulnerabilities of Historic Centres in Italy: Insights from the Tuscan Area. *J. Cult. Herit.* **2022**, *54*, 79–93. [CrossRef]
19. Chieffo, N.; Formisano, A. The Influence of Geo-Hazard Effects on the Physical Vulnerability Assessment of the Built Heritage: An Application in a District of Naples. *Buildings* **2019**, *9*, 26. [CrossRef]
20. Formisano, A.; Massimilla, A. A Novel Procedure for Simplified Nonlinear Numerical Modeling of Structural Units in Masonry Aggregates. *Int. J. Archit. Herit.* **2018**, *12*, 1162–1170. [CrossRef]
21. Wang, P.; Milani, G. Seismic Vulnerability Prediction of Masonry Aggregates: Iterative Finite Element Upper Bound Limit Analysis Approximating No Tensile Resistance. *Eng. Struct.* **2023**, *293*, 116595. [CrossRef]
22. Formisano, A.; Mochi, G.; Chieffo, N. Empirical and Mechanical Analysis Methods for Seismic Vulnerability Assessment of Clustered Buildings of Historical Centres: A Case Study. In Proceedings of the 8th International Conference on Computational Methods in Structural Dynamic Analysis and Its Application to Performance-Based Earthquake Engineering, Athens, Greece, 28–30 June 2021; pp. 28–30.
23. Greco, A.; Lombardo, G.; Pantò, B.; Famà, A. Seismic Vulnerability of Historical Masonry Aggregate Buildings in Oriental Sicily. *Int. J. Archit. Herit.* **2020**, *14*, 517–540. [CrossRef]
24. Grillanda, N.; Valente, M.; Milani, G.; Chiozzi, A.; Tralli, A. Advanced Numerical Strategies for Seismic Assessment of Historical Masonry Aggregates. *Eng. Struct.* **2020**, *212*, 110441. [CrossRef]

25. Mosoarca, M.; Onescu, I.; Onescu, E.; Azap, B.; Chieffo, N.; Szitar-Sirbu, M. Seismic Vulnerability Assessment for the Historical Areas of the Timisoara City, Romania. *Eng. Fail. Anal.* **2019**, *101*, 86–112. [CrossRef]
26. Penna, A.; Rosti, A.; Rota, M. Seismic Response of Masonry Building Aggregates in Historic Centres: Observations, Analyses and Tests. In *Seismic Behaviour and Design of Irregular and Complex Civil Structures IV*; Springer: Berlin/Heidelberg, Germany, 2022; pp. 19–36.
27. Cardinali, V.; Cristofaro, M.T.; Ferrini, M.; Nudo, R.; Paoletti, B.; Tanganelli, M. A Multiscale Approach for the Seismic Vulnerability Assessment of Historical Centres in Masonry Building Aggregates: Cognitive Approach and Interdisciplinary Perspectives. *Int. J. Archit. Herit.* **2022**, *16*, 839–864. [CrossRef]
28. Chieffo, N.; Formisano, A.; Lourenço, P.B. Seismic Vulnerability Procedures for Historical Masonry Structural Aggregates: Analysis of the Historical Centre of Castelpoto (South Italy). In Proceedings of the Structures; Elsevier: Amsterdam, The Netherlands, 2023; Volume 48, pp. 852–866.
29. Cocco, G.; D'Aloisio, A.; Spacone, E.; Brando, G. Seismic Vulnerability of Buildings in Historic Centers: From the "Urban" to the "Aggregate" Scale. *Front. Built Environ.* **2019**, *5*, 78. [CrossRef]
30. Valluzzi, M.R. *User Manual of Vulnus_4.0, Original Program by Bernardini Gori A, Modena R C, Vb Version Edited by Valluzzi MR, with Contributions by Benincà G, Barbetta E, Munari M*; Informer Technologies, Inc.: Los Angeles, CA, USA, 2009. (In Italian)
31. Benedetti, D.; Petrini, V. Sulla Vulnerabilita Sismica Di Edifici in Muratura: Proposta Su Un Metodo Di Valutazione. *l'Industria Costr.* **1984**, *149*, 66–74.
32. Formisano, A.; Mazzolani, F.M.; Florio, G.; Landolfo, R. A Quick Methodology for Seismic Vulnerability Assessment of Historical Masonry Aggregates. In Proceedings of the COST ACTION C26: Urban Habitat Constructions under Catastrophic Events-Proceedings of the Final Conference, Naples, Italy, 16–18 September 2010.
33. Formisano, A.; Florio, G.; Landolfo, R.; Mazzolani, F.M. Numerical Calibration of a Simplified Procedure for the Seismic Behaviour Assessment of Masonry Building Aggregates. In Proceedings of the 13th International Conference on Civil, Structural and Environmental Engineering Computing, Chania, Greece, 6–9 September 2011.
34. Lagomarsino, S.; Penna, A.; Galasco, A.; Cattari, S. TREMURI Program: An Equivalent Frame Model for the Nonlinear Seismic Analysis of Masonry Buildings. *Eng. Struct.* **2013**, *56*, 1787–1799. [CrossRef]
35. Porter, K. A Beginner's Guide to Fragility, Vulnerability, and Risk. In *Encyclopedia of Earthquake Engineering*; Springer: Berlin/Heidelberg, Germany, 2021.
36. Porter, K.; Kennedy, R.; Bachman, R. Creating Fragility Functions for Performance-Based Earthquake Engineering. *Earthq. Spectra* **2007**, *23*, 471–489. [CrossRef]
37. Angiolilli, M.; Brunelli, A.; Cattari, S. Fragility Curves of Masonry Buildings in Aggregate Accounting for Local Mechanisms and Site Effects. *Bull. Earthq. Eng.* **2023**, *21*, 2877–2919. [CrossRef]
38. Angiolilli, M.; Lagomarsino, S.; Cattari, S.; Degli Abbati, S. Seismic Fragility Assessment of Existing Masonry Buildings in Aggregate. *Eng. Struct.* **2021**, *247*, 113218. [CrossRef]
39. Cima, V.; Tomei, V.; Grande, E.; Imbimbo, M. Fragility Curves at Regional Basis for Unreinforced Masonry Buildings Prone to Out-of-Plane Mechanisms: The Case of Central Italy. *Structures* **2021**, *34*, 4774–4787. [CrossRef]
40. Simões, A.G.; Bento, R.; Lagomarsino, S.; Cattari, S.; Lourenço, P.B. Seismic Assessment of Nineteenth and Twentieth Centuries URM Buildings in Lisbon: Structural Features and Derivation of Fragility Curves. *Bull. Earthq. Eng.* **2020**, *18*, 645–672. [CrossRef]
41. Ruggieri, S.; Liguori, F.S.; Leggieri, V.; Bilotta, A.; Madeo, A.; Casolo, S.; Uva, G. An Archetype-Based Automated Procedure to Derive Global-Local Seismic Fragility of Masonry Building Aggregates: META-FORMA-XL. *Int. J. Disaster Risk Reduct.* **2023**, *95*, 103903. [CrossRef]
42. Maio, R.; Vicente, R.; Formisano, A.; Varum, H. Seismic Vulnerability of Building Aggregates through Hybrid and Indirect Assessment Techniques. *Bull. Earthq. Eng.* **2015**, *13*, 2995–3014. [CrossRef]
43. Sandoli, A.; Pacella, G.; Calderoni, B.; Brandonisio, G.; Lignola, G.P.; Prota, A. Predictive Hybrid Fragility Models for Urban Scale Seismic Assessment: A Case Study in Basilicata Region (Italy). *Bull. Earthq. Eng.* **2023**, *21*, 1047–1077. [CrossRef]
44. Sandoli, A.; Brandonisio, G.; Lignola, G.P.; Prota, A.; Fabbrocino, G. Seismic Fragility Matrices for Large Scale Probabilistic Structural Safety Assessment. *Soil. Dyn. Earthq. Eng.* **2023**, *171*, 107963. [CrossRef]
45. Cima, V.; Tomei, V.; Grande, E.; Imbimbo, M. Fragility Curves for the Seismic Assessment of Masonry Buildings in Historic Centres Prone to Out-of-Plane Failure Modes. *Bull. Earthq. Eng.* **2024**, *22*, 1801–1826. [CrossRef]
46. Cima, V.; Tomei, V.; Grande, E.; Imbimbo, M. Fragility Curves for Residential Unreinforced Masonry Buildings Prone to Out-of-Plane Mechanisms: The Case of the Historical Center of Sora. *Procedia Struct. Integr.* **2023**, *44*, 211–218. [CrossRef]
47. Cima, V.; Tomei, V.; Grande, E.; Imbimbo, M. An approach for deriving fragility curves of masonry buildings in aggregates. In Proceedings of the COMPDYN 2023 9th ECCOMAS Thematic Conference on Computational Methods in Structural Dynamics and Earthquake Engineering, Athens, Greece, 12–14 June 2023.
48. Casapulla, C.; Argiento, L.U. Non-Linear Kinematic Analysis of Masonry Walls out-of-Plane Loaded. The Comparative Role of Friction between Interlocked Walls. In Proceedings of the COMPDYN 2017 6th International Conference on Computational Methods in Structural Dynamics and Earthquake Engineering, Rhodes Island, Greece, 15–17 June 2017.
49. Casapulla, C.; Argiento, L.U.; Maione, A.; Speranza, E. Upgraded Formulations for the Onset of Local Mechanisms in Multi-Storey Masonry Buildings Using Limit Analysis. *Structures* **2021**, *31*, 380–394. [CrossRef]

50. ISR 2019 Italian Seismic Recommendations 2019. Circolare 21 Gennaio 2019 n.7: Istruzioni per l'applicazione Dell'«Aggiornamento Delle "Norme Tecniche per Le Costruzioni"» Di Cui al Decreto Ministeriale 17 Gennaio 2018. 2019. Available online: https://sttan.it/norme/NTC2018/NTC2018_Circ_21_01_2019_n7-CS_LL_PP.pdf (accessed on 29 March 2024).
51. Zuccaro, G.; Dolce, M.; Perelli, F.L.; De Gregorio, D.; Speranza, E. Cartis: A Method for the Typological-Structural Characterization of Italian Ordinary Buildings in Urban Areas. *Front. Built Environ.* **2023**, *9*, 1129176. [CrossRef]
52. Zuccaro, G.; Dolce, M.; De Gregorio, D.; Speranza, E.; Moroni, C. La Scheda CARTIS per La Caratterizzazione Tipologico-Strutturale Dei Comparti Urbani Costituiti Da Edifici Ordinari. Valutazione Dell'esposizione in Analisi Di Rischio Sismico. In Proceedings of the XXXIV National Conference of GNGTS, Trieste, Italy, 17–19 November 2015.
53. Protezione Civile Manual for the Compilation of the 1° Level Form for the Typological-Structural Characterization of Urban Sectors Consisting in Ordinary Buildings. 2017. Available online: http://plinivs.it/cartis/MANUALE_SCHEDA_CARTIS_eng_ottobre2021.pdf (accessed on 29 March 2024).
54. Saccucci, M.; Cima, V.; Grande, E.; Imimbo, M.; Pelliccio, A. The Knowledge Process in the Seismic Assessment of Masonry Building Aggregates—An Italian Case Study. In *International Conference on Critical Thinking in Sustainable Rehabilitation and Risk Management of the Built Environment*; Rotaru, A., Ed.; Springer: Cham, Germany, 2021; pp. 330–347. ISBN 978-3-030-61118-7.
55. CNR-DT212. Recommendations for the Probabilistic Seismic Assessment of Existing Buildings. 2013. Available online: https://www.airesingegneria.it/site/assets/files/1233/cnr_dt212_2013.pdf (accessed on 29 March 2024). (In Italian).
56. Giordano, N.; De Risi, R.; Voyagaki, E.; Kloukinas, P.; Novelli, V.; Kafodya, I.; Ngoma, I.; Goda, K.; Macdonald, J. Seismic Fragility Models for Typical Non-Engineered URM Residential Buildings in Malawi. In Proceedings of the Structures; Elsevier: Amsterdam, The Netherlands, 2021; Volume 32, pp. 2266–2278.
57. Heyman, J. The Stone Skeleton. *Int. J. Solids Struct.* **1966**, *2*, 249–279. [CrossRef]
58. Lagomarsino, S.; Resemini, S. The Assessment of Damage Limitation State in the Seismic Analysis of Monumental Buildings. *Earthq. Spectra* **2009**, *25*, 323–346. [CrossRef]
59. Casapulla, C.; Argiento, L.U. The Comparative Role of Friction in Local Out-of-Plane Mechanisms of Masonry Buildings. Pushover Analysis and Experimental Investigation. *Eng. Struct.* **2016**, *126*, 158–173. [CrossRef]
60. Spallarossa, D.; Barani, S. Disaggregazione Della Pericolosità Sismica in Termini Di MR-ε. Progetto DPC-INGV S1, Deliverable D14 2007. Available online: http://esse1.mi.ingv.it/d14.html (accessed on 29 March 2024).
61. Bazzurro, P.; Allin Cornell, C. Disaggregation of Seismic Hazard. *Bull. Seismol. Soc. Am.* **1999**, *89*, 501–520. [CrossRef]
62. *NTC18 Norme Tecniche per Le Costruzioni. DM 17/1/2018*; Italian Ministry of Infrastructure and Transport: Rome, Italy, 2018.
63. Fajfar, P. Capacity Spectrum Method Based on Inelastic Demand Spectra. *Earthq. Eng. Struct. Dyn.* **1999**, *28*, 979–993. [CrossRef]
64. Chichino, B.; Peloso, S.; Bolognini, D.; Moroni, C.; Perrone, D.; Brunesi, E. Towards Seismic Design of Nonstructural Elements: Italian Code-Compliant Acceleration Floor Response Spectra. *Adv. Civil. Eng.* **2021**, *2021*, 1–18. [CrossRef]
65. Lagomarsino, S.; Cattari, S. PERPETUATE Guidelines for Seismic Performance-Based Assessment of Cultural Heritage Masonry Structures. *Bull. Earthq. Eng.* **2015**, *13*, 13–47. [CrossRef]
66. Lagomarsino, S. Seismic Assessment of Rocking Masonry Structures. *Bull. Earthq. Eng.* **2015**, *13*, 97–128. [CrossRef]
67. D'Ayala, D.; Meslem, A.; Vamvatsikos, D.; Porter, K.; Rossetto, T. Guidelines for Analytical Vulnerability Assessment: Low/Mid-Rise, GEM Vulnerability and Loss Modelling. *Glob. Earthq. Model. GEM Found. Pavia* **2015**. Available online: https://discovery.ucl.ac.uk/id/eprint/10125202/1/GEM-GC-VLM-AVALMGuidelines-final.pdf (accessed on 20 December 2023).
68. Nielson, B.G.; DesRoches, R. Seismic Fragility Methodology for Highway Bridges Using a Component Level Approach. *Earthq. Eng. Struct. Dyn.* **2007**, *36*, 823–839. [CrossRef]
69. Jalayer, F.; De Risi, R.; Manfredi, G. Bayesian Cloud Analysis: Efficient Structural Fragility Assessment Using Linear Regression. *Bull. Earthq. Eng.* **2015**, *13*, 1183–1203. [CrossRef]
70. Lagomarsino, S.; Cattari, S. Fragility Functions of Masonry Buildings. *Geotech. Geol. Earthq. Eng.* **2014**, *27*, 111–156. [CrossRef]
71. Assunta, P.; Marco, S.; Ernesto, G. HT-BIM: Parametric Modelling for the Assessment of Risk in Historic Centers. *Disegnarecon* **2017**, *10*, 5.1–5.12.
72. Fragomeli, A.; Galasco, A.; Graziotti, F.; Guerrini, G.; Kallioras, S.; Magenes, G.; Malomo, D.; Mandirola, M.; Manzini, C.F.; Marchesi, B. Comportamento Degli Edifici in Muratura Nella Sequenza Sismica Dell'Italia Centrale Del 2016-Parte 2: Esempi Di Centri Colpiti. *Progett. Sismica* **2017**, *8*, 49–77.
73. Iervolino, I.; Galasso, C.; Cosenza, E. REXEL: Computer Aided Record Selection for Code-Based Seismic Structural Analysis. *Bull. Earthq. Eng.* **2010**, *8*, 339–362. [CrossRef]
74. Luzi, L.; Hailemikael, S.; Bindi, D.; Pacor, F.; Mele, F.; Sabetta, F. ITACA (ITalian ACcelerometric Archive): A Web Portal for the Dissemination of Italian Strong-Motion Data. *Seismol. Res. Lett.* **2008**, *79*, 716–722. [CrossRef]
75. Silvestri, F.; de Silva, F.; Piro, A.; Parisi, F. Soil-Structure Interaction Effects on out-of-Plane Seismic Response and Damage of Masonry Buildings with Shallow Foundations. *Soil. Dyn. Earthq. Eng.* **2024**, *177*, 108403. [CrossRef]